Inorganic Chemistry

Article

pubs.acs.org/IC

Combined Experimental and Computational Study of Pyren-2,7-diyl-Bridged Diruthenium Complexes with Various Terminal Ligands

Chang-Jiang Yao, Hai-Jing Nie, Wen-Wen Yang, Jiannian Yao, and Yu-Wu Zhong*

Beijing National Laboratory for Molecular Sciences, CAS Key Laboratory of Photochemistry, Institute of Chemistry, Chinese Academy of Sciences, 2 Bei Yi Jie, Zhong Guan Cun, Beijing 100190, People's Republic of China

Supporting Information

ABSTRACT: Cyclometalated diruthenium complexes $\mathbf{1}(PF_6)_2$–$\mathbf{5}(PF_6)_2$ bridged by 1,3,6,8-tetra(pyrid-2-yl)-pyrene have been prepared, with the terminal ligand bis(*N*-methylbenzimidazolyl)pyridine ($\mathbf{1}(PF_6)_2$), 4′-di-(*p*-methoxyphenyl)amino-2,2′:6′,2″-terpyridine ($\mathbf{2}(PF_6)_2$), 4′-*p*-methoxyphenyl-2,2′:6′,2″-terpyridine ($\mathbf{3}(PF_6)_2$), 2,2′:6′,2″-terpyridine ($\mathbf{4}(PF_6)_2$), and trimethyl-4,4′,4″-tricarboxylate-2,2′:6′,2″-terpyridine ($\mathbf{5}(PF_6)_2$). The single-crystal X-ray structure of $\mathbf{4}(PF_6)_2$ is presented. These complexes show two stepwise anodic redox pairs, and the potentials progressively increase from $\mathbf{1}(PF_6)_2$ to $\mathbf{5}(PF_6)_2$. Complexes $\mathbf{1}(PF_6)_2$–$\mathbf{4}(PF_6)_2$ have comparable electrochemical potential splitting of 200–210 mV, while complex $\mathbf{5}(PF_6)_2$ has a splitting of 170 mV. Upon one-electron oxidation by chemical oxidation or electrolysis, the resulting mixed-valent complexes $\mathbf{1}^{3+}$–$\mathbf{5}^{3+}$ display broad and intense absorptions between 1000 and 3000 nm. Complexes $\mathbf{1}^{3+}$ and $\mathbf{2}^{3+}$ show the presence of a higher-energy shoulder band in addition to the main near-infrared absorption band. This shoulder band is less distinguished for $\mathbf{3}^{3+}$–$\mathbf{5}^{3+}$. Three-state theory has been used to explain this difference. The one-electron oxidized forms, $\mathbf{1}^{3+}$–$\mathbf{5}^{3+}$, exhibit rhombic EPR signals at 77 K with the isotropic *g* values in the range of 2.18–2.24. Density functional theory (DFT) and time-dependent DFT (TDDFT) computations have been performed on $\mathbf{1}^{2+}$–$\mathbf{5}^{2+}$ to characterize their electronic structures and rationalize the absorption spectra in a wide energy range. DFT computations on $\mathbf{1}^{3+}$–$\mathbf{5}^{3+}$ show that both ruthenium ions and the bridging ligand have comparable spin densities. TDDFT computations on $\mathbf{1}^{3+}$ and $\mathbf{4}^{3+}$ have been performed to complement the experimental results.

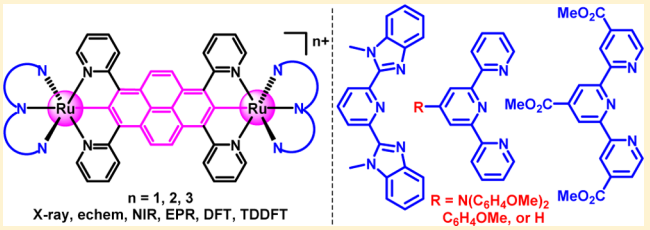

INTRODUCTION

Dimetallic complexes bridged by a π-conjugated component have been the focus of intensive research activities.[1] When the metal units undergo a chemically reversible redox process, a mixed-valence (MV) state can be generated, where individual metal units are in different oxidation states. Since the pioneering work of Creutz and Taube,[2] the MV chemistry has received tremendous interest in the last five decades.[1,3] These studies have been driven by the impetus to rationalize the charge delocalization between MV metal centers, which are of fundamental relevance to the naturally occurring photo-induced electron-transfer (ET) processes. In addition, complexes with well-defined redox processes are appealing materials for molecule-based electronics.[4] Numerous studies have demonstrated that such complexes display enhanced molecular conductance, and the conductance can be switched by manipulating the oxidation state of the molecular wire.[4]

When a moderate to strong electronic coupling is present between individual metal centers M_a and M_b of a MV complex, a metal-to-metal charge-transfer (MMCT) transition is often observed in the near-infrared (NIR) region. According to Marcus, Hush, and others, the electron coupling in a symmetric MV system can be rationalized on the basis of a classical two-state theory,[5] where the magnitude of the electronic coupling is defined by the matrix element $H_{ab} = \langle \psi_a | H | \psi_b \rangle$. In this description, H is the Hamiltonian operator and ψ_a and ψ_b represent two diabatic localized states, $[M_a^n\text{–BL–}M_b^{n+1}]$ and $[M_a^{n+1}\text{–BL–}M_b^n]$ (BL = bridging ligand). For a weak to moderate coupling (Robin–Day[6] class II) system, the interaction of two diabatic states gives rise to two new adiabatic potential energy surfaces along the asymmetric ET coordinate. The optically induced vertical transition from the energy minimum of the adiabatic ground state surface to the excited-state potential surface is the MMCT transition, and the energy of MMCT (E_{op}) equals the reorganization energy of the underlying ET process. The H_{ab} constant can be derived from the Hush formula[5] $H_{ab} = 0.0206(\varepsilon_{max}\nu_{max}\Delta\nu_{1/2})^{1/2}/(r_{ab})$. For a fully delocalized (class III) system, the interaction of $[M_a^n\text{–}BL\text{–}M_b^{n+1}]$ and $[M_a^{n+1}\text{–BL–}M_b^n]$ results in a ground-state potential surface with a single energy minimum and the H_{ab} value can be directly derived from $E_{op} = 2H_{ab}$.

Recently, a special type of redox-active dimetallic complexes has attracted considerable attention, where the metal centers are connected to the carbon-rich bridge with a metal–carbon bond.[7] As a result of the strong orbital overlap between the metal component and the BL, these systems often display strong metal–metal electronic coupling. However, when the

Received: December 30, 2014
Published: May 7, 2015

DOI: 10.1021/ic503117k
Inorg. Chem. 2015, 54, 4688–4698

metal-based and bridge-based redox orbitals are close in energy, the BL may become redox noninnocent.[8] In this case, a third state that explicitly allows for the active participation of the bridge, $[M_a^n-BL^+-M_b^n]$, should be invoked. Three-center models dealing with such open-shell systems have been known[9] and received much recent interest.[10] In addition to the asymmetric ET coordinate associated with the termini-localized states, a symmetric ET coordinate, perpendicular to the former one, is introduced to account for the charge transfer to/from the bridge. As result, a three-dimensional potential energy surface is envisaged. The position of the bridge state can be defined by an energy shift parameter Δ and a depth parameter d,[11] the latter corresponding to the position of the bridge state to the MV state along the symmetric ET coordinate. If $\Delta > 0$, the bridge state lies higher in energy than the MV state, and the electronic coupling among the $[M_a^n-BL-M_b^n]$ assembly brings about an adiabatic ground state and excited state involving M_a and M_b and a higher-energy excited state of BL character. In addition, two NIR transitions are predicted in this model, i.e., the MMCT and metal-to-bridge charge-transfer (MBCT) transitions.[10b,12] The MBCT must be higher in energy with respect to the MMCT. As the overall electronic coupling (including both donor–acceptor and donor–bridge coupling) increases, the MBCT band will increase in energy and the MMCT band decrease in energy. This occurs because increased coupling decreases the energy of the two metal-centered states and increases the energy of the mediating state.[10b] However, the energy change in the MMCT band is believed to be smaller with respect to that of the MBCT band. As a result, the energy difference between the MMCT and the MBCT bands increases. If $\Delta < 0$, the ground state is of bridge character, and the open-shell system can be treated as a bridge-based electrophore supported by two terminal metal units.[7h,8]

Although a number of three-state models have been proposed and validated, real systems can be more complicated and should be studied case by case. For instance, Low and co-workers recently reported a series of bimetallic ruthenium complexes $[\{Ru(dppe)Cp^*\}_2(\mu\text{-}C{\equiv}CArC{\equiv}C)]$ featuring di-ethynylaromatic bridging ligands[13] and found that the radical cation forms of these complexes exhibited simultaneous populations of bridge-localized and MV states. This phenomenon was thought to be caused by the presence of different orientations of the BL-based aromatic plane with respect to the metal d orbitals of appropriate symmetry. Kubiak and co-workers studied a series of pyrazine-bridged dimers of trinuclear ruthenium clusters with various terminal ligands.[12] Two distinct NIR bands were observed for these open-shell complexes, and the energies of these bands are greatly dependent on the electronic nature of terminal ligands. These two bands have been well explained by the MBCT and MMCT transitions of the three-state model.

Some time ago, we found that the reaction of $[Ru(tpy)Cl_3]$ (tpy = 2,2′:6′,2″-terpyridine) with 1,3,6,8-tetra(2-pyridyl)-pyrene ($tppyrH_2$) in the presence of AgOTf afforded a 2,7-diruthenium metalated pyrene complex, $[(tpy)Ru(tppyr)Ru(tpy)](PF_6)_2$ ($\mathbf{4}(PF_6)_2$ in Figure 1), in acceptable yield.[14] Complex $\mathbf{4}(PF_6)_2$ displays two well-separated anodic redox pairs, and the one-electron oxidized form exhibited a broad NIR absorption band around 2100 nm. This band was assigned as the MMCT transition of a MV state. Later studies demonstrated that similar diruthenium complexes containing a vinyl group on the terminal tpy ligands could be smoothly electropolymerized on electrode surfaces, and the resulting

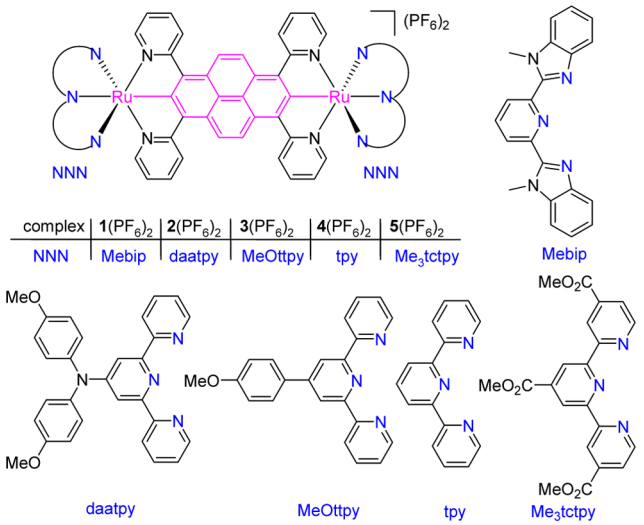

Figure 1. Compounds studied in this paper.

metallopolymeric films exhibited interesting electrochromism in the NIR region.[15] Being aware of the fact that the 2,7-bisanionic pyrene could be a redox noninnocent BL, we realized that the description of $\mathbf{4}^{3+}$ using a classical two-state model was possibly inappropriate. In order to clarify the nature of the one-electron oxidized forms of the 2,7-diruthenium metalated pyrene derivatives, we prepared and studied a series of related compounds, $\mathbf{1}(PF_6)_2$–$\mathbf{5}(PF_6)_2$, with terminal ligands of various electronic nature (Figure 1). Fortunately, a single crystal of $\mathbf{4}(PF_6)_2$ has been obtained. On the basis of its molecular structure obtained from X-ray analysis (Figure 2), density functional theory (DFT) and time-dependent DFT

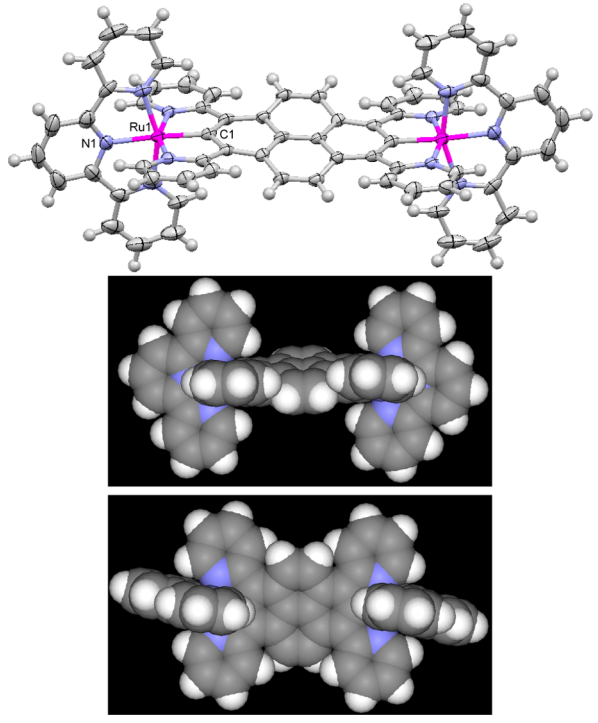

Figure 2. Thermal ellipsoid diagram (30% probability) and CPK models of the single-crystal structure of $\mathbf{4}(PF_6)_2$. Anions are omitted for clarity. Atom color code: carbon, gray; nitrogen, blue; ruthenium, magenta.

DOI: 10.1021/ic503117k
Inorg. Chem. 2015, 54, 4688–4698

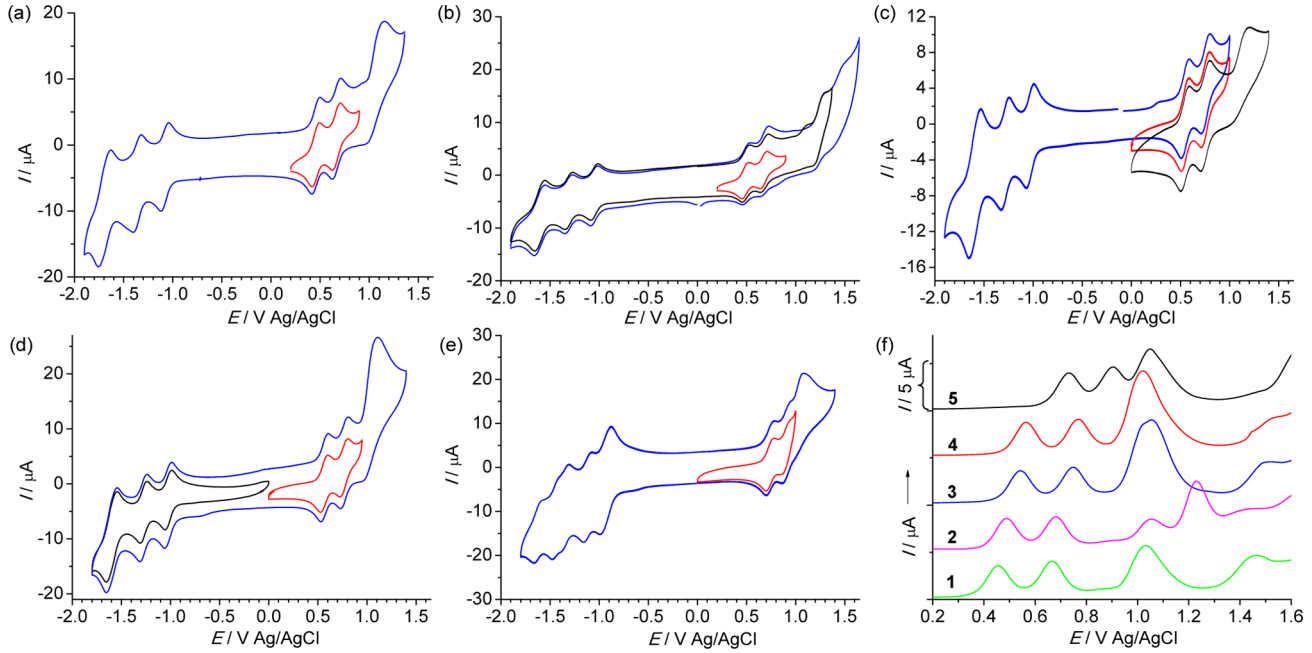

Figure 3. (a–e) CVs of $\mathbf{1}(PF_6)_2$–$\mathbf{5}(PF_6)_2$ and (f) anodic DPVs of $\mathbf{1}(PF_6)_2$–$\mathbf{5}(PF_6)_2$ at 100 mV/s in 0.1 M $^nBu_4NClO_4$/DMF.

Table 1. Electrochemical and Absorption Data[a]

compound	$E_{1/2}$ (anodic)	ΔE^c (mV)	$E_{1/2}$ (cathodic)	λ_{max}/nm (ε/10^5 M^{-1} cm^{-1})[d]
$\mathbf{1}(PF_6)_2$	+0.46, +0.67, +1.15[b]	210	−1.08, −1.36, −1.70	334(1.17), 348(1.06), 467(0.46), 508(0.71), 706(0.23), 798(0.097)
$\mathbf{2}(PF_6)_2$	+0.48, +0.68, +1.03,[b] +1.24[b]	200	−1.05, −1.32, −1.61	286(0.94), 312(1.09), 338(0.97), 430(0.32), 456(0.47), 486(0.63), 598(0.43), 642(0.51), 804(0.085)
$\mathbf{3}(PF_6)_2$	+0.54, +0.75, +1.18[b]	210	−1.04, −1.28, −1.60	284(0.81), 322(1.08), 426(0.25), 452(0.39), 484(0.56), 586(0.42), 628(0.44), 768(0.082)
$\mathbf{4}(PF_6)_2$	+0.56, +0.76, +1.11[b]	200	−1.03, −1.27, −1.59	278(0.82), 318(1.33), 424(0.27), 452(0.46), 482(0.66), 586(0.43), 624(0.42), 760(0.10)
$\mathbf{5}(PF_6)_2$	+0.74, +0.91, +1.07[b]	170	−0.93, −1.12, −1.34, −1.45, −1.63	294(0.77), 325(0.85), 440(0.47), 470(0.49), 613(0.59)

[a]The potential is reported as the $E_{1/2}$ value vs Ag/AgCl unless otherwise noted. [b]Irreversible oxidation, E_{anodic}. [c]ΔE is the potential difference between the first and the second anodic process. [d]Absorption data in CH_3CN.

(TDDFT) computations have been performed on $\mathbf{1}^{2+}$–$\mathbf{5}^{2+}$ and the corresponding one-electron oxidized forms, $\mathbf{1}^{3+}$–$\mathbf{5}^{3+}$. A combined experimental and computational study of the diruthenium complexes $\mathbf{1}^{n+}$–$\mathbf{5}^{n+}$ (n = 2, 3) is presented in this contribution.

RESULTS AND DISCUSSION

Synthesis of Diruthenium Complexes and Single-Crystal X-ray Analysis of $\mathbf{4}(PF_6)_2$. According to the known procedures[16] for the synthesis of cyclometalated ruthenium complexes, $\mathbf{1}(PF_6)_2$–$\mathbf{5}(PF_6)_2$ were prepared from the reaction of the neutral ligand tppyrH$_2$[14] with various [Ru(L)Cl$_3$] salt in the presence of AgOTf, followed by anion exchange using KPF_6, where L = bis(*N*-methylbenzimidazolyl)pyridine (Mebip),[17] 4′-di-(*p*-methoxyphenyl)amino-2,2′:6′,2″-terpyridine (daatpy),[18] 4′-*p*-methoxyphenyl-2,2′:6′,2″-terpyridine (MeOttpy), tpy, and trimethyl-4,4′,4″-tricarboxylate-2,2′:6′,2″-terpyridine (Me_3tc-tpy).[19] Ligands Mebip and daatpy are electron donating, while Me_3tctpy is electron deficient. Ligands tpy and MeOttpy have intermediate properties. These ligands were deliberately selected in order to systematically examine the electronic properties of the resulting complexes. We were pleased to find that five diruthenium complexes could be successfully obtained in acceptable yields using a common procedure, irrespective of the electronic nature of the terminal ligands. The characterization data of $\mathbf{4}(PF_6)_2$ has been previously reported.[14] Others are provided in the Experimental Section.

A single crystal of $\mathbf{4}(PF_6)_2$ suitable for X-ray analysis was obtained by slow diffusion of diethyl ether into a solution of $\mathbf{4}(PF_6)_2$ in CH_3CN.[20] The thermal ellipsoid diagram and CPK models are shown in Figure 2. The structure is C_2 symmetric. The Ru–C bond (Ru1–C1) is 1.954(5) Å in length. The Ru–N bond opposite to the cyclometalated bond is 2.018(4) Å. Other Ru–N bonds are in the range of 2.07–2.09 Å. The two Ru ions have a geometrical separation of 10.979 Å. The central naphthalene unit has a good planar structure, which has a torsion angle of 16.1(8)° with respect to the neighboring pyridine rings. This can be clearly seen from the CPK models. The two cyclometalating phenyl rings are slightly twisted to fit for this torsion.

Electrochemical Studies. The electronic properties of the above complexes were studied by cyclic voltammetric (CV) analysis. All complexes show two well-defined anodic redox pairs (Figure 3 and Table 1) in dimethylformamide (DMF), and the redox potentials are greatly dependent on the terminal ligands. Complexes $\mathbf{1}(PF_6)_2$ and $\mathbf{2}(PF_6)_2$ with electron-donating terminal ligands show waves at less positive potentials

DOI: 10.1021/ic503117k
Inorg. Chem. 2015, 54, 4688–4698

[+0.46 and +0.67 V vs Ag/AgCl for $\mathbf{1}(PF_6)_2$; +0.48 and +0.68 V for $\mathbf{2}(PF_6)_2$]. Complex $\mathbf{5}(PF_6)_2$ with electron-deficient Me_3tctpy ligands shows waves at more positive potentials (+0.74 and +0.91 V). Complexes $\mathbf{1}(PF_6)_2$–$\mathbf{4}(PF_6)_2$ have comparable electrochemical potential splitting of 200–210 mV, while complex $\mathbf{5}(PF_6)_2$ has a relatively smaller splitting of 170 mV. The peak-to-peak potential difference of each redox couple is around 60–70 mV, in good agreement with the one-electron Nernstian process (the theoretical value is 59 mV). The redox potentials of these waves become increasingly positive from $\mathbf{1}(PF_6)_2$ to $\mathbf{5}(PF_6)_2$. This trend can be clearly seen from the differential pulse voltammograms (PDVs) shown in Figure 3f. These waves are assigned to the $Ru^{III/II}$ processes mixing with some amount of oxidation of the BL.[16−19] At more positive potentials, these complexes show some quasi-reversible or irreversible anodic waves which are likely associated with the ligand-based oxidative decompositions or the $Ru^{IV/III}$ processes, as have been found in many cyclometalated ruthenium complexes.[16−19] For the daatpy-terminated complex $\mathbf{2}(PF_6)_2$, the oxidations of the amine units of the terminal ligands are likely involved in the region between +1.0 and +1.5 V. The amine oxidation of the daatpy ligand itself occurs at +0.99 V vs Ag/AgCl.[21] After coordinating with the ruthenium component, it is reasonable that the amine oxidations shifted to a more positive potential region.

The two-step oxidation events for these complexes are also evident in a slightly less positive potential region in the electrochemical measurements in CH_3CN, as shown in the CVs of $\mathbf{2}(PF_6)_2$, $\mathbf{4}(PF_6)_2$, and $\mathbf{5}(PF_6)_2$ in Figures S1–S3, Supporting Information. However, these complexes have somewhat limited solubility in CH_3CN in the presence of electrolyte. DMF is thus a better choice as the solvent for the electrochemical measurements.

In the cathodic scans of $\mathbf{1}(PF_6)_2$–$\mathbf{4}(PF_6)_2$, three redox couples are observed for each complex. The first two waves are associated with the reductions of the BL, and the third one is from the terminal ligands. This is supported by the later DFT studies, which indicate that the LUMO of these complexes is associated with the BL. The terminal ligands make major contributions to the higher-lying unoccupied orbitals. Complex $\mathbf{5}(PF_6)_2$ with Me_3tctpy displays multiple cathodic waves because each Me_3tctpy unit is able to accept more than one electron. The first cathodic wave is best assigned as a two-electron reduction of Me_3tctpy judging from its higher peak currents relative to the next one. A previously reported cyclometalated monoruthenium complex $[Ru(Me_3tctpy)(dpb)](PF_6)_2$ (dpb = 1,3-di(pyrid-2-yl)benzene) also shows two cathodic waves at −1.10 and −1.46 V vs Ag/AgCl, while related complex $[Ru(tpy)(dpb)](PF_6)_2$ only shows one cathodic wave at a similar potential region.[16g]

Electronic Absorption Spectra. The electronic absorption spectra of $\mathbf{1}(PF_6)_2$–$\mathbf{5}(PF_6)_2$ were recorded in CH_3CN (Figure 4). The absorption maxima and molar extinction data are given in Table 1. The absorptions in the ultraviolet (UV) region are due to intraligand transitions from both the BL and the terminal ligands. In the visible (vis) to NIR region, three main absorption bands are distinguished: one with three sub-bands between 400 and 520 nm, one broad band around 520–720 nm, and another separate band around 760 nm. For complex $\mathbf{5}(PF_6)_2$, the third low-energy band appears as a shoulder band around 720 nm. The assignment of these bands will be further discussed in the later TDDFT discussions.

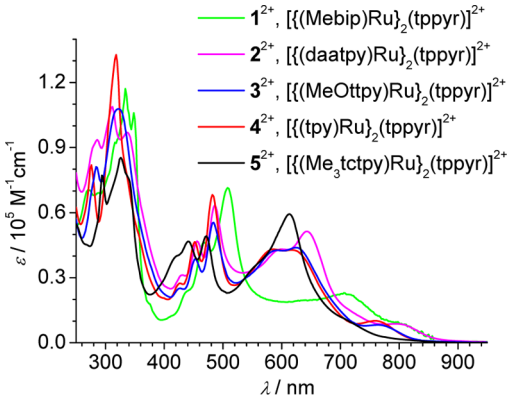

Figure 4. UV–vis spectra of $\mathbf{1}(PF_6)_2$–$\mathbf{5}(PF_6)_2$ in acetonitrile.

Oxidative Titration. The stepwise oxidations of $\mathbf{4}(PF_6)_2$ have previously been performed using bromine, and a broad absorption band between 1000 and 3000 nm was observed for the one-electron oxidized form $\mathbf{4}^{3+}$.[14a] This band was not present in $\mathbf{4}^{2+}$ and the dioxidized $\mathbf{4}^{4+}$. Herein, we present the spectroscopic studies of $\mathbf{1}^{2+}$–$\mathbf{5}^{2+}$ upon oxidative titration with cerium ammonium nitrate (CAN) in CH_3CN (Figures 5 and S4, Supporting Information). This reagent is easier to handle than bromine, and the equivalent of the oxidant can be precisely controlled.[22]

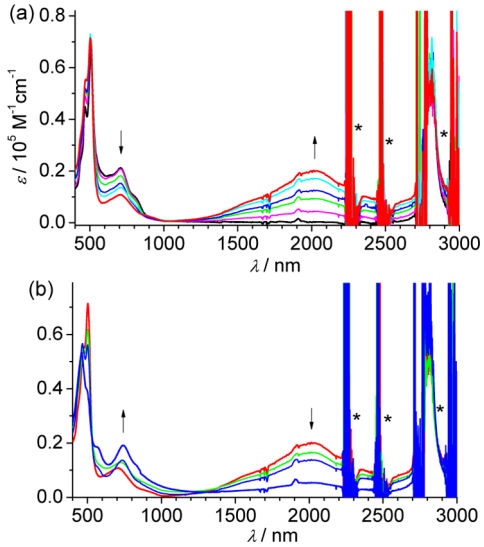

Figure 5. Absorption spectral changes of $\mathbf{1}(PF_6)_2$ (1×10^{-5} M in CH_3CN) during stepwise (a) one-electron oxidation and (b) second one-electron oxidation by chemical oxidations using CAN. Asterisk (*) indicates artifacts.

All complexes displayed similar spectral changes during these processes. When up to 1 equiv of CAN was added, a broad absorption band in the NIR region gradually increased. Upon the second one-electron oxidation, this NIR band decreased. Apparently, these NIR bands are only associated with the one-electron oxidized forms, $\mathbf{1}^{3+}$–$\mathbf{5}^{3+}$. However, the shapes of these NIR bands show some difference among each complex. The NIR bands of $\mathbf{1}^{3+}$ and $\mathbf{2}^{3+}$ clearly consist of two subcomponents. They can be well fitted by two Gaussian functions (Figure 6a and 6b), with a shoulder band around 6500 cm^{-1} in addition to the main absorption around 5000 cm^{-1}. For complexes $\mathbf{3}^{3+}$–$\mathbf{5}^{3+}$, the higher-energy shoulder band is less distinct. The NIR

DOI: 10.1021/ic503117k
Inorg. Chem. 2015, 54, 4688–4698

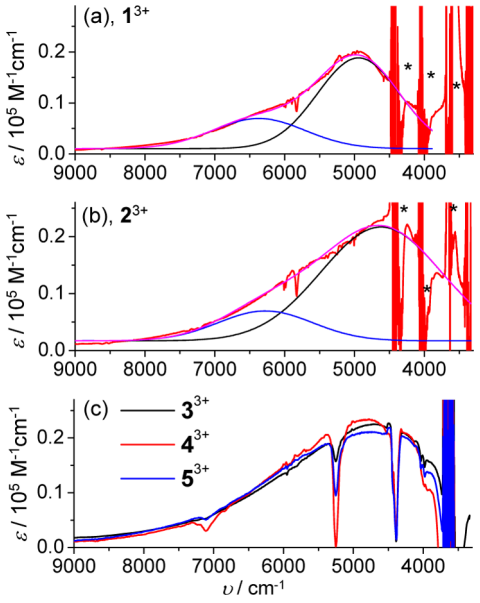

Figure 6. NIR spectra versus wavenumbers (υ) of the one-electron oxidized forms, $\mathbf{1}^{3+}$–$\mathbf{5}^{3+}$ (obtained by oxidation with CAN in CH_3CN; 1×10^{-5} M for $\mathbf{1}^{3+}$ and $\mathbf{2}^{3+}$; 5×10^{-5} M for $\mathbf{3}^{3+}$–$\mathbf{5}^{3+}$; shape and energy of the NIR transitions are independent of the concentration). Spectra of $\mathbf{1}^{3+}$ and $\mathbf{2}^{3+}$ were deconvoluted into two Gaussian functions. Asterisk (*) indicates artifacts.

transitions of $\mathbf{3}^{3+}$–$\mathbf{5}^{3+}$ are asymmetric, being broader on the high-energy side and steeper on the low-energy side.

MV compounds can display multiple NIR absorption bands (instead of one intervalence charge transfer band) for a number of reasons. The first one could be the presence of a strong spin–orbit coupling, which allows transitions from other metal d orbitals (especially for the third-low transition metal complexes) to be observed in the NIR region.[23] Since the spin–orbit coupling for ruthenium is relatively small, this is very likely not the case for $\mathbf{1}^{3+}$ and $\mathbf{2}^{3+}$.

We consider that the higher-energy shoulder band of $\mathbf{1}^{3+}$ and $\mathbf{2}^{3+}$ is possibly of the MBCT character, and the main absorptions belong to the MMCT transitions. This interpretation is in accordance with the main characteristic of the MBCT transitions,[10b,12] namely, the MBCT must be higher in energy relative to the MMCT band. The above electrochemical studies indicated that the potential splitting ΔE values are essentially the same for $\mathbf{1}(PF_6)_2$–$\mathbf{4}(PF_6)_2$ (200 or 210 mV). Complex $\mathbf{5}(PF_6)_2$ has the relatively smaller ΔE value (170 mV). This may suggest that complex $\mathbf{5}(PF_6)_2$ has the smallest electronic coupling among five complexes. We note that ΔE depends on a variety of different factors except the electronic coupling, such as electrostatic effect, inductive contribution, and measurement conditions.[24] For a series of structurally related complexes, it may be qualitatively true. However, as judging from Figure 6, the intensity of the NIR bands of each complex is very similar and the difference of the electronic coupling should be small.

The three-state theory suggests that as the overall electronic coupling increases, the MBCT band will increase in energy, the MMCT band will slightly decrease in energy, and the energy separation between them will increase.[10b,12] Figure 6 shows that complexes $\mathbf{4}^{3+}$–$\mathbf{5}^{3+}$ have similar NIR absorption energy, while the main absorption of $\mathbf{1}^{3+}$ (assigned as the MMCT band) is slightly higher in energy with respect to those of $\mathbf{4}^{3+}$–$\mathbf{5}^{3+}$. For complexes $\mathbf{1}^{3+}$ and $\mathbf{2}^{3+}$, the slightly stronger coupling makes the MBCT and MMCT separable, which is consistent with the three-state theory. For the other three complexes, the NIR absorption may contain overlapping MMCT and MBCT bands.

Another possibility of the higher-energy shoulder bands of $\mathbf{1}^{3+}$ and $\mathbf{2}^{3+}$ could be due to vibronic coupling. The energy separation between the two NIR bands of $\mathbf{1}^{3+}$ and $\mathbf{2}^{3+}$ is around 1300–1500 cm^{-1}. Vibronic coupling of similar frequency has been previously reported for strongly coupled organic MV systems, while it is often not found in inorganic MV compounds.[25]

On the basis of the deconvoluted MMCT bands, the metal–metal electronic coupling parameters of $\mathbf{1}^{3+}$ and $\mathbf{2}^{3+}$ were determined to be 700 and 870 cm^{-1}, according to the Hush formula $H_{ab} = 0.0206 \times (\varepsilon_{max}\nu_{max}\Delta\nu_{1/2})^{1/2}/(r_{ab})$,[5] where ν_{max} is the energy of the MMCT band and r_{ab} is the electron transfer distance. The r_{ab} value was estimated by the Ru–Ru geometrical distance (10.98 Å), which is very likely longer with respect to the real electron transfer distance due to charge delocalization.[3m–o]

In principle, the stepwise oxidations could also be performed by an electrochemical method. For example, Figure S5, Supporting Information, shows the absorption spectral changes of $\mathbf{4}(PF_6)_2$ in CH_2Cl_2 upon electrolysis using an indium–tin–oxide (ITO) glass electrode. The appearance and disappearance of the NIR bands are also evident during the mono- and dioxidation processes. Figure S6, Supporting Information, displays the NIR bands of $\mathbf{2}^{3+}$ and $\mathbf{4}^{3+}$ obtained after electrolysis in different solvents of varied polarity (CH_2Cl_2, CH_3CN, and DMF). Both compounds have small solvatochromic effects in terms of band energies and shapes, which suggests that they are strongly coupled systems. Complexes $\mathbf{1}^{2+}$, $\mathbf{3}^{2+}$, and $\mathbf{5}^{2+}$ have limited solubility in the above solvents in the presence of electrolyte, and the spectroelectrochemical measurements of these three complexes have not been performed.

Figure S7, Supporting Information, shows a comparison of the NIR absorption spectra of $\mathbf{4}^{3+}$ obtained by electrolysis of $\mathbf{4}(PF_6)_2$ in Bu_4NClO_4/CH_3CN or chemical oxidation using CAN. In the electrolysis case, the counteranions of $\mathbf{4}^{3+}$ are mostly from the electrolyte solution, namely, ClO_4^-. In the chemical oxidation case, the anions of $\mathbf{4}^{3+}$ contain both PF_6^- and NO_3^-. The NIR spectra obtained by two methods are very similar. This means that the use of CAN for the stepwise oxidation is reliable and the NIR spectra of $\mathbf{4}^{3+}$ are not sensitive to anions. This conclusion may apply to other four diruthenium complexes with different terminal ligands.

EPR Studies. EPR spectroscopy is a useful tool for analyzing spin density distributions of metal complexes with a redox noninnocent ligand.[7,8,26] A free organic spin has a g factor g_e = 2.0023. A low-spin Ru^{III} (d^5) atom often exhibits a rhombic or axial EPR signal at low temperature as solid or frozen solutions. The deviation of the isotropic g factor $\langle g \rangle$ ($= [(g_1^2 + g_2^2 + g_3^2)/3]^{1/2}$) from g_e and the anisotropy Δg ($= g_1 - g_3$) reflect the spin density distributions among the metal and ligand components and the symmetry at the metal center as a result of spin–orbital coupling and low-symmetry ligand-field effects.

Complexes $\mathbf{1}^{3+}$–$\mathbf{5}^{3+}$ are EPR inactive at room temperature. At 77 K in frozen CH_3CN, they display rhombic signals (Figure 7). The samples were obtained after adding 0.5 equiv of CAN to $\mathbf{1}(PF_6)_2$–$\mathbf{5}(PF_6)_2$ in CH_3CN and used for EPR measurements directly. The $\langle g \rangle$ and Δg values of each complex are summarized in Table 2. As has been pointed out above, rhombic signals are typical for a low-spin Ru(III) species.

DOI: 10.1021/ic503117k
Inorg. Chem. 2015, 54, 4688–4698

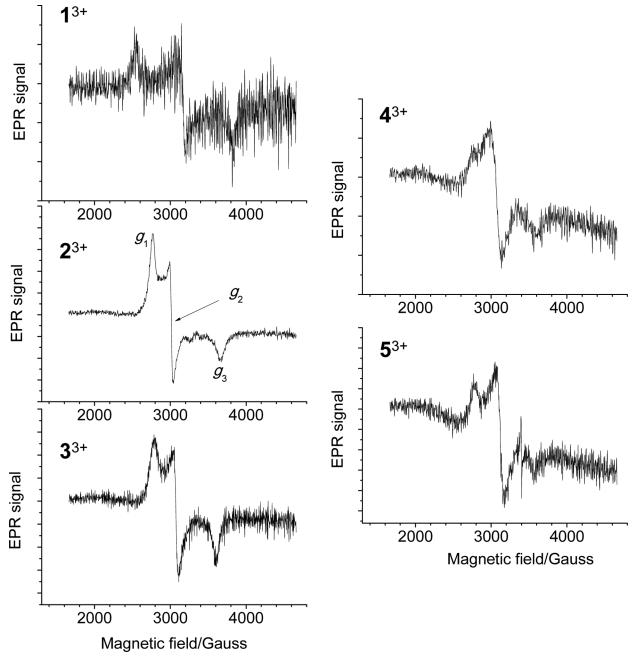

Figure 7. EPR spectra of $\mathbf{1}^{3+}$−$\mathbf{5}^{3+}$ in acetonitrile at 77K.

Table 2. EPR Data[a]

	$\mathbf{1}^{3+}$	$\mathbf{2}^{3+}$	$\mathbf{3}^{3+}$	$\mathbf{4}^{3+}$	$\mathbf{5}^{3+}$
g_1	2.6787	2.4579	2.4414	2.4581	2.4480
g_2	2.1533	2.2589	2.2090	2.2124	2.1750
g_3	1.7767	1.8554	1.8863	1.8888	1.9036
$\langle g \rangle$	2.2337	2.2050	2.1907	2.1987	2.1867
Δg	0.9020	0.6025	0.5551	0.5693	0.5444

[a] $\langle g \rangle = [(g_1^2 + g_2^2 + g_3^2)/3]^{1/2}$. $\Delta g = g_1 - g_3$.

However, the average $\langle g \rangle$ values (2.18−2.24) of $\mathbf{1}^{3+}$−$\mathbf{5}^{3+}$ are all significantly smaller than a reported true ruthenium-centered spin of a catecholatoruthenium(III) complex ($\langle g \rangle$ = 2.476).[27] This could be caused by considerable distributions of the spin density in the pyrene framework of $\mathbf{1}^{3+}$−$\mathbf{5}^{3+}$. Similar EPR analysis has been used by Kaim and Lahiri for the estimation of the participation of a ligand in redox processes.[27] Another feature is that the Δg value of $\mathbf{1}^{3+}$ is distinctly larger and the Δg value of $\mathbf{2}^{3+}$ is slightly larger relative to those of $\mathbf{3}^{3+}$−$\mathbf{5}^{3+}$. This trend can indeed be correlated to the above NIR spectra, where the spectrum of $\mathbf{1}^{3+}$ is also significantly different from those of $\mathbf{3}^{3+}$−$\mathbf{5}^{3+}$ and complex $\mathbf{2}^{3+}$ represents an intermediate situation. This may suggest that the weight of the unpaired spin density on the ruthenium centers versus the BL is higher for $\mathbf{1}^{3+}$ and $\mathbf{2}^{3+}$ with respect to that of the other three complexes.

FTIR Spectra of $\mathbf{5}^{n+}$. Figure S8, Supporting Information, shows the FTIR spectra of $\mathbf{5}^{2+}$, $\mathbf{5}^{3+}$, and $\mathbf{5}^{4+}$. They display a signal carbonyl peak at the same wavenumbers (1730 cm^{-1}). The change of the redox state of the molecule seems to have little influence on the vibration energy of the carbonyl group of Me_3tctpy of **5**.

DFT and TDDFT Computations of $\mathbf{1}^{2+}$−$\mathbf{5}^{2+}$. DFT calculations have been performed on $\mathbf{1}^{2+}$−$\mathbf{5}^{2+}$ using the Gaussian 09 package.[28] The input files were generated starting from the single-crystal structure of $\mathbf{4}^{2+}$. The hybrid B3LYP exchange correlation functional[29] with the LANL2DZ basis set[30] for ruthenium and 6-31G* for other atoms[31] were used. The computations were carried out taking into account solvation effects by means of the conductor polarizable continuum model (CPCM)[32] in CH_3CN solution.

Five types of frontier orbital compositions are commonly predicted for all complexes. Taking $\mathbf{4}^{2+}$ as an example (Figure 8), the ruthenium ions and the bis(cyclometalating) pyrene

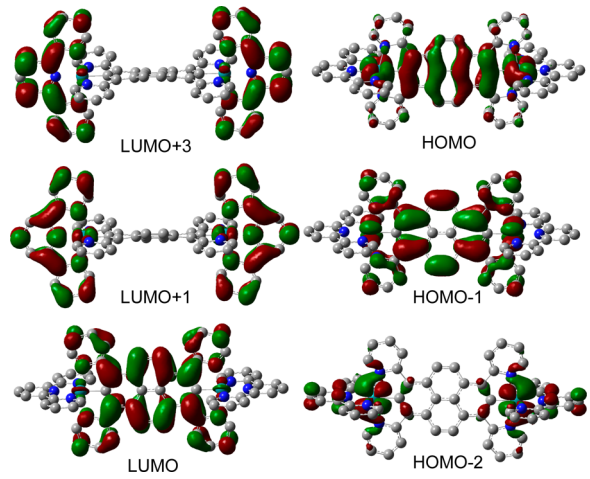

Figure 8. Isodensity plots of selected frontier orbitals of $\mathbf{4}^{2+}$.

bridge equally contribute to the HOMO. Similar HOMO compositions have previously been found for many bridged bimetallic cyclometalated complexes.[7] The LUMO and HOMO-1 of $\mathbf{4}^{2+}$ resemble the LUMO and HOMO of the pristine pyrene (Figure S9, Supporting Information), respectively, with little involvement of the ruthenium ions. An anodal plane structure across the 2,7 positions of pyrene is evident for those orbitals. The higher-lying unoccupied orbitals of $\mathbf{4}^{2+}$, such as LUMO+1, LUMO+2, LUMO+3, and LUMO+4, are dominated by the terminal ligands. The lower-lying occupied orbitals, such as, HOMO-2, HOMO-3, and HOMO-4, are mainly of ruthenium character.

Figure S10, Supporting Information, shows the energy diagram of complexes computed. The orbital isodensity plots are provided in Figures S11−S15, Supporting Information. For the frontier unoccupied orbitals, complexes $\mathbf{1}^{2+}$−$\mathbf{3}^{2+}$ basically have the same orbital orderings and compositions as $\mathbf{4}^{2+}$. However, the Me_3tctpy-terminated complex $\mathbf{5}^{2+}$ shows a difference. The electron-withdrawing Me_3tctpy groups are responsible for the quasi-degenerate LUMO and LUMO+1 orbitals, which are slightly more stabilized with respect to the pyrene-dominated orbital, LUMO+2. For the frontier occupied orbitals, complexes $\mathbf{1}^{2+}$, $\mathbf{3}^{2+}$, and $\mathbf{5}^{2+}$ all have a similar set of frontier orbitals as $\mathbf{4}^{2+}$. The daatpy-terminated complex $\mathbf{2}^{2+}$ is slightly different. Two ruthenium-dominated orbitals, with some contributions from the triarylamine units, are lifted to HOMO-1 and HOMO-2. The pyrene-dominated occupied orbital is lowered to HOMO-3.

The HOMOs of all complexes have very similar compositions and even contributions from the whole [Ru−pyrene−Ru] array. In general, complexes with electron-donating terminal ligands show relatively destabilized HOMO levels (−4.88, −4.85, −4.95, −4.98, and −5.20 eV for $\mathbf{1}^{2+}$, $\mathbf{2}^{2+}$, $\mathbf{3}^{2+}$, $\mathbf{4}^{2+}$, and $\mathbf{5}^{2+}$, respectively), and complex $\mathbf{5}^{2+}$ with the electron-withdrawing ligand Me_3tctpy has the most stabilized HOMO level. This trend is in accordance with the electrochemical results shown in Figure 3. However, the triarylamine-containing complex $\mathbf{2}^{2+}$ seems to be an exception. The HOMO

DOI: 10.1021/ic503117k
Inorg. Chem. 2015, 54, 4688−4698

Table 3. Calculated Spin Density Populations[a]

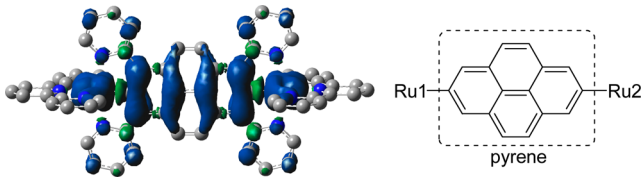

method	UB3LYP/CH_3CN					UB3LYP/H_2O		UCAM-B3LYP/CH_3CN			
compound	1^{3+}	2^{3+}	3^{3+}	4^{3+}	5^{3+}	1^{3+}	4^{3+}	1^{3+}	2^{3+}	4^{3+}	5^{3+}
Ru1	0.325	0.344	0.327	0.327	0.306	0.325	0.327	0.306	0.313	0.300	0.275
Ru2	0.325	0.337	0.329	0.327	0.306	0.325	0.327	0.306	0.315	0.300	0.275
pyrene	0.311	0.282	0.309	0.297	0.360	0.311	0.297	0.350	0.337	0.349	0.420
(Ru1 + Ru2)/pyrene	2.09	2.41	2.12	2.20	1.98	2.09	2.20	1.75	1.86	1.72	1.31

[a]Spin density is determined by the difference of the Mulliken charges of α and β electrons ($\alpha - \beta$). The spin density plots are provided in Figure S17, Supporting Information.

of 2^{2+} lies slightly higher in energy than that of 1^{2+}, but the latter is slightly easier to be oxidized. The calculated Mulliken populations of the HOMOs of 1^{2+}–5^{2+} are summarized in Table S1, Supporting Information. The ruthenium ions and the pyrene backbone have comparable contributions for all complexes. For instance, in the HOMO of 1^{2+}, each ruthenium atom and the pyrene component have a Mulliken population of 0.23 and 0.38, respectively. These values vary slightly for other complexes. As for the pyrene component itself, the two cyclometalating phenyl rings make major contributions.

To assist the assignment of the visible absorptions, TDDFT calculations were performed on 1^{2+}, 4^{2+}, and 5^{2+} on the above optimized structures using the same level of theory. Predicted electronic transitions are shown in Figure S16, Supporting Information, and details of these excitations are given in Table S2, Supporting Information. Frontier orbitals involved in these transitions are given in Figures S11, S14, and S15, Supporting Information. In general, TDDFT-predicted excitations are somewhat blue shifted with respect to the absorption spectra. However, the shapes and relative oscillator strengths (f) of the predicted excitations agree well with the experimental data.

Taking complex 4^{2+} as an example, the separate band at 760 nm is associated with the HOMO → LUMO excitation (the S_1 excitation at 683 nm, f = 0.1161), which can be interpreted as the mixed character of the metal-to-ligand charge-transfer (MLCT) transitions from the ruthenium atoms to pyrene and the intraligand charge transfer of the pyrene fragment. The broad band between 520 and 720 nm is mainly associated with the HOMO-1 → LUMO excitation (the S_4 excitation at 584 nm, f = 1.0196) and is a result of the pyrene-localized excitation mixing with some amount of MLCT transitions. The absorptions between 400 and 520 nm are of MLCT character from the HOMO-5 and HOMO-6, targeting at both the BL and the terminal ligands (LUMO, LUMO+3, and LUMO+4, associated with the S_{17} and S_{24} excitations).

The predicted excitations of 1^{2+} and 5^{2+} suggest very similar assignments for their absorptions. However, the predicted S_1 excitation (HOMO → LUMO) of 5^{2+} has a very low f value of 0.0024, which indeed agrees with the absence of a separate low-energy absorption band of this complex. It should be noted that these low-energy distinct absorption bands of complexes 1^{2+}–4^{2+} are quite unusual for polypyridine ruthenium complexes. To the best of our knowledge, only a bimetallic cyclometalated ruthenium bridged by 1,3,4,6-tetra(2-pyridyl)benzene, reported recently by us,[7g] shows a similar low-energy absorption band of HOMO → LUMO character.

DFT and TDDFT Computations of 1^{3+}–5^{3+}. In the studies of open-shell compounds with redox-active ligands,[7,8] DFT and TDDFT computations are very helpful in elucidating the spin density distributions and the nature of NIR absorptions.[33] On the basis of the previous DFT-optimized structures of 1^{2+}–5^{2+}, the structures of the mono-oxidized forms, 1^{3+}–5^{3+}, were reoptimized at the level of theory of UB3LYP/LANL2DZ/6-31G*/CPCM/CH_3CN) by changing the charges to 3 and multiplicities to 2. The optimized structures of 1^{3+}–5^{3+} are still C_2 symmetric (Table S3, Supporting Information). The Ru–C bond of each complex becomes 0.03–0.04 Å shorter after one-electron oxidation. The pyrene backbone also shows some slight structural changes.

The calculated Mulliken spin density distributions of these open-shell substances are shown in Figure S17, Supporting Information, and summarized in Table 3. One common feature is that all complexes have comparable spin density populations among the [Ru–pyrene–Ru] array, and the two ruthenium ions of individual complexes essentially have equal contributions. However, the ratio of (Ru1 + Ru2)/pyrene varies slightly among each complex. Complex 2^{3+} with the electron-donating daatpy ligand has the largest (Ru1 + Ru2)/pyrene ratio (2.41), while complex 5^{3+} with the electron-withdrawing ligand Me_3tctpy has the smallest (Ru1 + Ru2)/pyrene ratio (1.98). Although this difference is not significant, it indeed partially coincides with the above EPR results, which shows that complexes with electron-donating terminal ligands have slightly bigger g anisotropy and complexes with electron-withdrawing terminal ligands have slightly smaller g anisotropy. One exception is complex 1^{3+}. Nevertheless, the DFT results should be taken with care due to its overestimation of charge delocalization.[34]

Complexes 1^{3+} and 4^{3+} have also been calculated in aqueous solution.[35] The results are exactly the same as those calculated in CH_3CN (Table 3). We also performed the DFT calculations of 1^{3+}, 2^{3+}, 4^{3+}, and 5^{3+} with the long-range-corrected version of UB3LYP, UCAM-B3LYP,[36] in CH_3CN. Again, the two ruthenium ions of all complexes are calculated to have the same spin density contributions, and complex 5^{3+} with the electron-withdrawing ligand Me_3tctpy has the smallest (Ru1 + Ru2)/pyrene ratio (1.31). By comparing the results calculated using UB3LYP versus UCAM-B3LYP, the latter functional generally gives rise to smaller (Ru1 + Ru2)/pyrene ratios for

DOI: 10.1021/ic503117k
Inorg. Chem. 2015, 54, 4688–4698

the same complex. In addition, these calculation results suggest that the unpaired spin density in these open-shell complexes is delocalized across the whole [Ru−pyrene−Ru] array and can be slightly tuned by the electronic nature of the terminal ligands.

TDDFT calculations were performed on complexes $\mathbf{1}^{3+}$ and $\mathbf{4}^{3+}$ on the basis of the previous optimized structures to assist the assignments of their NIR absorptions (TDDFT calculations were always performed on the DFT-optimized structures with the same functionals and multiplicity). Predicted low-energy excitations of $\mathbf{4}^{3+}$ are given in Table 4. Involved spin orbitals are shown in Figure 9. In the NIR region, only one excitation, the D_2 (D = doublet) excitation at 2510.3 nm, is predicted for $\mathbf{4}^{3+}$ to have a strong oscillator strength (f = 0.4551). Other low-energy excitations have very low strengths. This is in accordance with the experimental observed spectrum centered at 2100 nm. This excitation is dominated by the β spin excitation from the highest occupied spin orbital (HOSO) to the lowest unoccupied spin orbital (LUSO), which has the in-phase and out-of-phase combination of the Ru d orbitals, respectively. This can be interpreted as the MMCT transitions. The D_4 and D_5 have some character of MBCT transitions, but the oscillator strengths are much lower with respect to that of D_2.

Table 4. TDDFT-Predicted Doublet (D) Low-Energy Excitations of $\mathbf{4}^{3+}$ [a]

D_n	λ/nm	f	dominant transitions (configuration coefficient)
1	2841.0	0.0000	β-HOSO-1 → β-LUSO (90%)
2	2510.3	0.4551	β-HOSO → β-LUSO (95%)
3	1941.8	0.0000	β-HOSO-2 → β-LUSO (98%)
4	1930.9	0.0040	β-HOSO-3 → β-LUSO (98%)
5	1768.4	0.0008	β-HOSO-4 → β-LUSO (98%)
6	1370.0	0.0000	β-HOSO-5 → β-LUSO (88%)
7	804.7	0.0037	β-HOSO-1 → β-LUSO+1 (43%)

[a]Computed at the level of TDDFT/B3LYP/LANL2DZ/6-31G*/CPCM/CH_3CN.

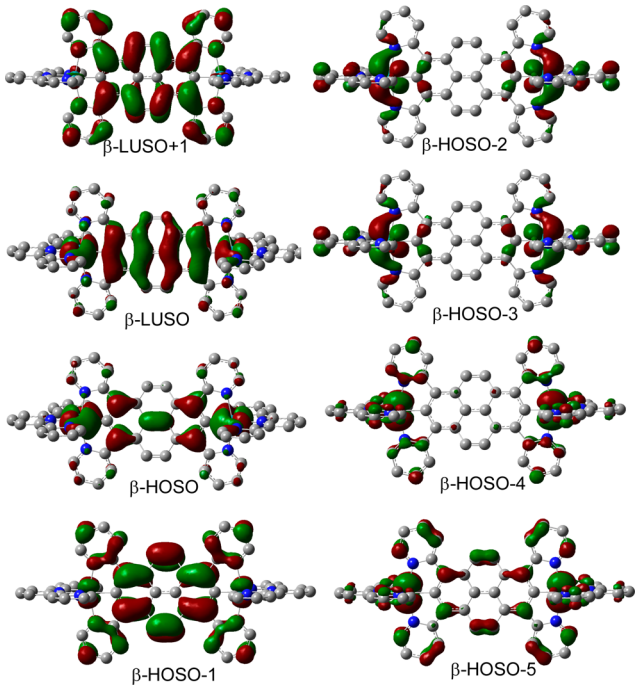

Figure 9. Spin orbitals and TDDFT-predicted excitations of $\mathbf{4}^{3+}$. See details in Table 4.

For complex $\mathbf{1}^{3+}$, the MMCT transition has been predicted at 2496.6 nm with the same HOSO → LUSO spin excitation (D_2, f = 0.4360, Table S4 and Figure S18, Supporting Information). Again, the D_5 excitation has some character of MBCT transitions (HOSO-5 → LUSO), but the oscillator strength (f = 0.0022) is much lower with respect to that of D_2.

CONCLUSION

In conclusion, a series of tppyr-bridged diruthenium complexes $\mathbf{1}(PF_6)_2$−$\mathbf{5}(PF_6)_2$, with various terminal ligands of different electronic nature, has been prepared through the double C−H bond activations of $tppyrH_2$. These complexes display two stepwise and well-separated anodic redox pairs. The potentials of these waves progressively increase from $\mathbf{1}(PF_6)_2$ to $\mathbf{5}(PF_6)_2$ as a result of the increasing electron-withdrawing nature of the terminal ligands.

The mono-oxidized forms, $\mathbf{1}^{3+}$−$\mathbf{5}^{3+}$, display rhombic EPR signals with relatively low $\langle g \rangle$ and Δg values, which suggests that the spin density populations in these complexes are more biased toward the ruthenium ions. However, considerable amounts of spin density are believed to be associated with the pyrene segment. This is supported by computational results. DFT studies of $\mathbf{1}^{3+}$−$\mathbf{5}^{3+}$ show that the ruthenium atoms and pyrene segment have comparable spin densities, and the spin density populations vary slightly with different terminal ligands. Using the three-state model language,[11] the energy shift parameters Δ are small positive values, and both ruthenium ions and the BL are responsible for the one-electron oxidation event.

Several studies on the influence of peripheral ligands on the electronic properties of MV compounds have been reported previously;[27c] however, a similar study on compounds with redox noninnocent BL has received less attention.[37] This study shows that the NIR transitions of the dicyclometalated complexes $\mathbf{1}^{3+}$−$\mathbf{5}^{3+}$ are slightly dependent on the electronic nature of the terminal ligands. With electron-donating terminal ligands ($\mathbf{1}^{3+}$ and $\mathbf{2}^{3+}$), two sub-bands can be distinguished. The higher-energy shoulder band can be either caused by the MBCT transitions or by the vibronic coupling. For the other three complexes, this shoulder band is less distinct and the NIR transitions appear as a highly asymmetric band. The possible MBCT band is too weak to be distinguished for $\mathbf{3}^{3+}$−$\mathbf{5}^{3+}$ or severely overlaps with the MMCT band.

EXPERIMENTAL SECTION

Spectroscopic Measurements. UV−vis−NIR spectra were recorded using a PerkinElmer Lambda 750 UV/vis/NIR spectrophotometer at room temperature in denoted solvents, with a conventional 1.0 cm quartz cell.

Electrochemical Measurement. All cyclic voltammetry measurements were taken using a CHI 660D potentiostat with a one-compartment electrochemical cell under an atmosphere of nitrogen. All measurements were carried out at a scan rate of 100 mV/s in denoted solvent containing 0.1 M of Bu_4NClO_4 as the supporting electrolyte. The working electrode was glassy carbon with a diameter of 3.0 mm. The electrode was polished prior to use with 0.05 μm alumina and rinsed thoroughly with water and acetone. A large-area platinum wire coil was used as the counter electrode. All potentials are

DOI: 10.1021/ic503117k
Inorg. Chem. 2015, 54, 4688−4698

referenced to a Ag/AgCl electrode in saturated aqueous NaCl without regard for the liquid junction potential.

Oxidative Spectroelectrochemistry. Oxidative spectroelectrochemistry was performed in a thin layer cell (optical length = 0.2 cm) in which an ITO glass electrode was set in indicated solvent containing 0.1 M Bu_4NClO_4 and the compound to be measured (the concentration is around 5×10^{-5} M). A platinum wire and Ag/AgCl in saturated aqueous solution was used as a counter electrode and a reference electrode. The cell was put into a PE Lambda 750 UV/vis/NIR spectrophotometer to monitor spectral changes during electrolysis.

X-ray Crystallography. The X-ray diffraction data were collected using a Rigaku Saturn 724 diffractometer on a rotating anode (Mo Kα radiation, λ = 0.71073 Å). The structure was solved by the direct method using SHELXS-97 and refined anisotropically on F^2 with SHELXL-97.

EPR Measurements. EPR Measurements were performed on a Bruker ELEXSYS E500-10/12 spectrometer at 77 K. The spectrometer frequency ν is 9.51×10^9 Hz. The mono-oxidized forms $\mathbf{1}^{3+}$–$\mathbf{5}^{3+}$ were obtained by adding 0.5 equiv of CAN to $\mathbf{1}^{2+}$–$\mathbf{5}^{2+}$ in CH_3CN in a NMR tube, and these samples were directly used for EPR measurements.

FTIR Measurements. FTIR measurements were performed in KBr pellets using a Bruker Tensor-27 spectrometer. Samples $\mathbf{5}^{3+}$ and $\mathbf{5}^{4+}$ were obtained by oxidation of $\mathbf{5}^{2+}$ with 1 or 2 equiv of cerium ammonium nitrate.

Computational Methods. DFT calculations were carried out using the B3LYP exchange correlation functional[29] or CAM-B3LYP functional[36] and implemented in the Gaussian 09 package.[28] The electronic structures of complexes were determined using a general basis set with the Los Alamos effective core potential LANL2DZ basis set for ruthenium[30] and 6-31G* for other atoms.[31] In all calculations, solvation effects are included, and the conductor-like polarizable continuum model (CPCM) was employed.[32] No symmetry constraints were used in the optimization (nosymm keyword was used). Frequency calculations have been performed with the same level of theory to ensure the optimized geometries to be local minima. All orbitals have been computed at an isovalue of 0.02 e/bohr^3.

Synthesis. NMR spectra were recorded in the designated solvent on a Bruker Avance 400 MHz spectrometer. Spectra are reported in ppm values from residual protons of deuterated solvent. Mass data were obtained with a Bruker Daltonics Inc. Apex II FT-ICR or Autoflex III MALDI-TOF mass spectrometer. The matrix for MALDI-TOF measurement is α-cyano-4-hydroxycinnamic acid. Microanalysis was carried out using Flash EA 1112 or Carlo Erba 1106 analyzer at the Institute of Chemistry, Chinese Academy of Sciences.

General Procedure for the Synthesis of Complexes $\mathbf{1}(PF_6)_2$–$\mathbf{5}(PF_6)_2$. To 20 mL of dry acetone were added 0.06 mmol of $[Ru(L)Cl_3]$ (L = terminal ligand) and AgOTf (0.2 mmol, 52 mg). The mixture was refluxed for 3 h before cooling to room temperature. The white AgCl precipitate was removed by filtering through a pad of Celite, and the filtrate was concentrated to dryness. To the residue were added $tppyrH_2$[14] (0.03 mmol, 15.4 mg), 10 mL of DMF, and 10 mL of ^{t}BuOH. The solution was transferred to a pressure vessel and bubbled with nitrogen for 20 min before the vial was capped and heated at 130 °C for 48 h. After cooling to room temperature, the solvent was removed under reduced pressure. The residue was dissolved in 2 mL of methanol. After adding an excess of KPF_6, the resulting precipitate was collected by filtering and washing with water and Et_2O. The crude solid was purified through flash column chromatography (eluent: CH_3CN/aq KNO_3/H_2O, 100/1/5) on silica gel, followed by anion exchange using KPF_6, to give the desired bisruthenium complex in acceptable yield. The characterization data of $\mathbf{4}(PF_6)_2$ has been reported previously.[14]

*[{(Mebip)Ru}$_2$(tppyr)](PF$_6$)$_2$ (**1**(PF$_6$)$_2$).* Yield: 65%. ^{1}H NMR (400 MHz, CD_3COCD_3): δ 4.65 (s, 12H), 6.66 (d, J = 12.8 Hz, 4H), 7.09 (d, J = 12.8 Hz, 4H), 7.61 (m, 12H), 7.88 (d, J = 8.4 Hz, 4H), 7.95 (d, J = 8.0 Hz, 4H), 8.00 (t, J = 8.2 Hz, 4H), 8.69 (d, J = 8.0 Hz, 4H), 8.87 (d, J = 8.4 Hz, 2H), 8.97 (d, J = 8.0 Hz, 4H). MALDI-MS: 1533.4 for $[M - PF_6 - 2H]^+$, 1373.4 for $[M - 2PF_6 - CH_3 - 2H]^+$. MALDI-HRMS calcd for $C_{78}H_{54}F_6N_{14}PRu_2$: 1535.2413. Found: 1535.2412. Anal. Calcd for $C_{78}H_{54}F_{12}N_{14}P_2Ru_2 \cdot Et_2O \cdot 4H_2O$: C, 53.95; H, 3.98; N, 10.74. Found: C, 54.33; H, 4.02; N, 10.31.

*[{(daatpy)Ru}$_2$(tppyr)](PF$_6$)$_2$ (**2**(PF$_6$)$_2$).* Yield: 66%. ^{1}H NMR (400 MHz, CD_3COCD_3): δ 3.93 (s, 12H), 6.95 (t, J = 6.4 Hz, 4H), 6.99 (t, J = 6.2 Hz, 4H), 7.15 (d, J = 5.2 Hz, 4H), 7.18 (d, J = 8.8 Hz, 8H), 7.59 (d, J = 9.2 Hz, 8H), 7.70 (t, J = 7.8 Hz, 4H), 7.75 (d, J = 5.2 Hz, 4H), 7.94 (t, J = 8.1 Hz, 4H), 8.32 (s, 4H), 8.37 (d, J = 8.0 Hz, 4H), 9.09 (d, J = 8.4 Hz, 4H), 9.43 (s, 4H). MALDI-MS: 1774.6 for $[M - PF_6]^+$, 1630.7 for $[M - 2PF_6]^+$. Anal. Calcd for $C_{94}H_{68}F_{12}N_{12}O_4P_2Ru_2$: C, 58.75; H, 3.57; N, 8.75. Found: C, 58.52; H, 3.58; N,8.30.

*[{(MeOttpy)Ru}$_2$(tppyr)](PF$_6$)$_2$ (**3**(PF$_6$)$_2$).* Yield: 42%. ^{1}H NMR (400 MHz, CD_3COCD_3): δ 4.01 (s, 6H), 6.95 (t, J = 6.4 Hz, 4H), 7.08 (t, J = 6.4 Hz, 4H), 7.31 (m, 8H), 7.62 (d, J = 5.2 Hz, 4H), 7.88 (t, J = 7.8 Hz, 4H), 7.95 (t, J = 7.6 Hz, 4H), 8.37 (d, J = 8.4 Hz, 4H), 9.00 (d, J = 8.0 Hz, 4H), 9.12 (d, J = 8.4 Hz, 4H), 9.43 (s, 4H), 9.48 (s, 4H). MALDI-MS: 1533.9 for $[M - PF_6 - H]^+$, 1389.0 for $[M - 2PF_6 - H]^+$. MALDI-HRMS calcd for $C_{80}H_{54}F_6N_{10}O_2PRu_2$: 1535.21901. Found: 2535.21898. Anal. Calcd for $C_{80}H_{54}F_{12}N_{10}O_2P_2Ru_2 \cdot 3H_2O$: C, 55.43; H, 3.49; N, 8.08. Found: C, 55.31; H, 3.71; N, 7.98.

*[{(Me$_3$tctpy)Ru}$_2$(tppyr)](PF$_6$)$_2$ (**5**(PF$_6$)$_2$).* Yield: 30%. ^{1}H NMR (400 MHz, CD_3CN): δ 3.86 (s, 12H), 4.23 (s, 6H), 6.75 (t, J = 6.6 Hz, 4H), 7.10 (d, J = 5.3 Hz, 4H), 7.41 (d, J = 5.7 Hz, 4H), 7.48 (d, J = 5.8 Hz, 4H), 7.84 (t, J = 7.4 Hz, 4H), 8.93 (d, J = 8.2 Hz, 4H), 9.09 (s, 4H), 9.35 (s, 4H), 9.50 (s, 4H). MALDI-MS: 1669.7 for $[M - PF_6 - H]^+$, 1524.9 for $[M - 2PF_6 - H]^+$. 1018.1 for $[M - 2PF_6 - Me_3tctpy - H]^+$. MALDI-HRMS calcd for $C_{78}H_{54}F_6N_{10}O_{12}PRu_2$: 1671.1682. Found: 1671.1690. Anal. Calcd for $C_{78}H_{54}F_{12}N_{10}P_2Ru_2 \cdot 2Et_2O \cdot H_2O$: C, 52.12; H, 3.87; N, 7.07. Found: C, 51.86; H, 3.81; N, 7.19.

■ ASSOCIATED CONTENT

Supporting Information

Cyclic voltammograms of $\mathbf{2}(PF_6)_2$, $\mathbf{4}(PF_6)_2$, and $\mathbf{5}(PF_6)_2$ in CH_3CN, absorption spectral changes of $\mathbf{1}(PF_6)_2$–$\mathbf{5}(PF_6)_2$ upon stepwise chemical oxidation, spectral changes of $\mathbf{4}^{2+}$ upon electrolysis, absorption spectra of $\mathbf{2}^{3+}$ and $\mathbf{4}^{3+}$ in different solvents, FTIR spectra of $\mathbf{5}^{2+}$, $\mathbf{5}^{3+}$, and $\mathbf{5}^{4+}$, DFT and TDDFT results, Cartesian coordinates of DFT-optimized structures, NMR and mass spectra of new compounds, and cif file of $\mathbf{4}(PF_6)_2$. The Supporting Information is available free of charge on the ACS Publications website at DOI: 10.1021/ic503117k.

■ AUTHOR INFORMATION

Corresponding Author

*E-mail: zhongyuwu@iccas.ac.cn.

Notes

The authors declare no competing financial interest.

■ ACKNOWLEDGMENTS

We thank the National Natural Science Foundation of China (grants 21271176, 91227104, 21472196, and 21221002), the National Basic Research 973 program of China (grant 2011CB932301), the Ministry of Science and Technology of China (grant 2012YQ120060), and the Strategic Priority Research Program of the Chinese Academy of Sciences (grant XDB 12010400) for funding support.

■ REFERENCES

(1) (a) D'Alessandro, D. M.; Keene, F. R. *Chem. Rev.* **2006**, *106*, 2270. (b) Kaim, W.; Lahiri, G. K. *Angew. Chem., Int. Ed.* **2007**, *46*, 1778. (c) Aguirre-Etcheverry, P.; O'Hare, D. *Chem. Rev.* **2010**, *110*, 4839. (d) Chisholm, M. H.; Lear, B. J. *Chem. Soc. Rev.* **2011**, *40*, 5254.

(2) Creutz, C.; Taube, H. *J. Am. Chem. Soc.* **1969**, *91*, 3988.

(3) (a) Pratt, R. C.; Lyons, C. T.; Wasinger, E. C.; Stack, T. D. P. *J. Am. Chem. Soc.* **2012**, *134*, 7367. (b) Xi, B.; Liu, I. P.-C.; Xu, G.-L.;

DOI: 10.1021/ic503117k
Inorg. Chem. 2015, 54, 4688–4698

Choudhuri, M. M. R.; DeRosa, M. C.; Crutchley, R. J.; Ren, T. *J. Am. Chem. Soc.* **2011**, *133*, 15094. (c) Kurahashi, T.; Fujii, H. *J. Am. Chem. Soc.* **2011**, *133*, 8307. (d) Bunting, P.; Chisholm, M. H.; Gallucci, J. C.; Lear, B. J. *J. Am. Chem. Soc.* **2011**, *133*, 5873. (e) Nemykin, V. N.; Rohde, G. T.; Barrett, C. D.; Hadt, R. G.; Bizzarri, C.; Galloni, P.; Floris, B.; Nowik, I.; Herber, R. H.; Marrani, A. G.; Zanoni, R.; Loim, N. M. *J. Am. Chem. Soc.* **2009**, *131*, 14969. (f) Heckmann, A.; Lambert, C. *Angew. Chem., Int. Ed.* **2012**, *51*, 326. (g) Hankache, J.; Wenger, O. S. *Chem. Rev.* **2011**, *111*, 5138. (h) Hildebrandt, A.; Rüffer, T.; Erasmus, E.; Swarts, J. C.; Lang, H. *Organometallics* **2010**, *29*, 4900. (i) Hildebrandt, A.; Lang, H. *Dalton Trans.* **2011**, *40*, 11831. (j) Choudhuri, M. M. R.; Kaim, W.; Sarkar, B.; Crutchley. *Inorg. Chem.* **2013**, *52*, 11060. (k) Sakamoto, R.; Tsukada, S.; Nishihara, H. *Dalton Trans.* **2012**, *41*, 10123. (l) Rao, K. P.; Kusamoto, T.; Toshimitsu, F.; Inayoshi, K.; Kume, S.; Sakamoto, R.; Nishihara, H. *J. Am. Chem. Soc.* **2010**, *132*, 12472. (m) Bublitz, G. U.; Laidlaw, W. M.; Denning, R. G.; Boxer, S. G. *J. Am. Chem. Soc.* **1998**, *120*, 6068. (n) Oh, D. H.; Sano, M.; Boxer, S. G. *J. Am. Chem. Soc.* **1991**, *113*, 6880. (o) Silverman, L. N.; Kanchanawong, P.; Treynor, T. P.; Boxer, S. G. *Philos. Trans. R. Soc. A* **2008**, *366*, 33.

(4) (a) Akita, M.; Koike, T. *Dalton Trans.* **2008**, 3523. (b) Tuccitto, N.; Ferri, V.; Cavazzini, M.; Quici, S.; Zhavnerko, G.; Licciardello, A.; Rampi, M. A. *Nat. Mater.* **2009**, *8*, 41. (c) Ying, J.-W.; Liu, I. P.-C.; Xi, B.; Song, Y.; Campana, C.; Zuo, J.-L.; Ren, T. *Angew. Chem., Int. Ed.* **2010**, *49*, 954. (d) Luo, L.; Renameur, A.; Brignou, P.; Choi, S. H.; Rigaut, S.; Frisbie, C. D. *J. Phys. Chem. C* **2011**, *115*, 19955. (e) Launay, J.-P. *Coord. Chem. Rev.* **2013**, *257*, 1544. (f) Sakamoto, R.; Katagiri, S.; Maeda, H.; Nishihara, H. *Coord. Chem. Rev.* **2013**, *257*, 1493. (g) Maeka, H.; Sakamoto, R.; Nishihara, H. *Chem.—Eur. J.* **2014**, *20*, 2761. (h) Kohler, L.; Kaveevivitchai, N.; Zong, R.; Thummel, R. P. *Inorg. Chem.* **2014**, *53*, 912.

(5) (a) Mulliken, R. S. *J. Am. Chem. Soc.* **1952**, *64*, 811. (b) Marcus, R. A. *Annu. Rev. Phys. Chem.* **1964**, *15*, 155. (c) Hush, N. S. *Prog. Inorg. Chem.* **1967**, *8*, 391. (d) Hush, N. S. *Coord. Chem. Rev.* **1985**, *64*, 135.

(6) Robin, M. B.; Day, P. *Adv. Inorg. Chem. Radiochem.* **1967**, *8*, 357.

(7) (a) Sutter, J.-P.; Grove, D. M.; Beley, M.; Collin, J.-P.; Veldman, N.; Spek, A. L.; Sauvage, J.-P.; van Koten, G. *Angew. Chem., Int. Ed.* **1994**, *33*, 1282. (b) Patoux, C.; Launay, J.-P.; Beley, M.; Chodorowski-Kimmers, S.; Collin, J.-P.; James, S.; Sauvage, J.-P. *J. Am. Chem. Soc.* **1998**, *120*, 3717. (c) Ren, T. *Organometallics* **2005**, *24*, 4854. (d) Low, P. J.; Roberts, R. L.; Cordiner, R. L.; Hartl, F. *J. Solid State Electrochem.* **2005**, *9*, 717. (e) Low, P. J.; Brown, N. J. *J. Cluster Sci.* **2010**, *21*, 235. (f) Costuas, K.; Rigaut, S. *Dalton Trans.* **2011**, *40*, 5643. (g) Yao, C.-J.; Zhong, Y.-W.; Yao, J. *J. Am. Chem. Soc.* **2011**, *133*, 15697. (h) Man, W. Y.; Xia, J.-L.; Brown, N. J.; Farmer, J. D.; Yufit, D. S.; Howard, J. A. K.; Liu, S. H.; Low, P. J. *Organometallics* **2011**, *30*, 1852. (i) Fitzgerald, E. C.; Brown, N. J.; Edge, R.; Helliwell, M.; Roberts, H. N.; Tuna, F.; Beeby, A.; Collison, D.; Low, P. J.; Whiteley, M. W. *Organometallics* **2011**, *30*, 157. (j) Pevny, F.; Di Piazza, E.; Norel, L.; Drescher, M.; Winter, R. F.; Rigaut, S. *Organometallics* **2010**, *29*, 5912. (k) Hoffert, W. A.; Rappé, A. K.; Shores, M. P. *J. Am. Chem. Soc.* **2011**, *133*, 20823. (l) Olivier, C.; Costuas, K.; Choua, S.; Maurel, V.; Turek, P.; Saillard, J.-Y.; Touchard, D.; Rigaut, S. *J. Am. Chem. Soc.* **2010**, *132*, 5638. (m) Wadman, S. H.; Havenith, R. W. A.; Lutz, M.; Spek, A. L.; van Klink, G. P. M.; van Koten, G. *J. Am. Chem. Soc.* **2010**, *132*, 1914.

(8) (a) Ward, M. D.; McCleverty, J. A. *J. Chem. Soc., Dalton Trans.* **2002**, 275. (b) Lever, A. B. P.; Gorelsky, S. I. *Struct. Bonding (Berlin)* **2004**, *107*, 77. (c) Boyer, J. L.; Rochford, J.; Tsai, M.-K.; Muckerman, J. T.; Fujita, E. *Coord. Chem. Rev.* **2010**, *254*, 309. (d) Lever, A. B. P. *Coord. Chem. Rev.* **2010**, *254*, 1397. (e) Dzik, W. I.; van der Vlugt, J. I.; Reek, J. N. H.; de Bruin, B. *Angew. Chem., Int. Ed.* **2011**, *50*, 3356. (f) Kaim, W. *Inorg. Chem.* **2011**, *50*, 9752. (g) Maurer, J.; Linseis, M.; Sarkar, B.; Schwederski, B.; Niemeyer, M.; Kaim, W.; Záliš, S.; Anson, C.; Zabel, M.; Winter, F. *J. Am. Chem. Soc.* **2008**, *130*, 259. (h) Das, A. K.; Sarkar, B.; Fiedler, J.; Zális, S.; Hartenbach, I.; Strobel, S.; Lahiri, G. K.; Kaim, W. *J. Am. Chem. Soc.* **2009**, *131*, 8895. (i) Gagliardo, M.; Amijs, C. H. M.; Lutz, M.; Spek, A. L.; Havenith, R. W. A.; Hartl, F.; van Klink, G. P. M.; van Koten, G. *Inorg. Chem.* **2007**, *46*, 11133. (j) Lohan, M.; Justaud, F.; Lang, H.; Lapinte, C. *Organometallics* **2012**, *31*, 3565. (k) Linseis, M.; Záliš, S.; Zabel, M.; Winter, R. F. *J. Am. Chem. Soc.* **2012**, *134*, 16671.

(9) (a) Piepho, S. B.; Krausz, E. R.; Schatz, P. N. *J. Am. Chem. Soc.* **1978**, *100*, 2996. (b) Root, L. J.; Ondrenchen, M. J. *Chem. Phys. Lett.* **1982**, *93*, 421. (c) Ondrenchen, M. J.; Ko, J.; Zhang, L. T. *J. Am. Chem. Soc.* **1987**, *109*, 1672. (d) Petrov, V.; Hupp, J. T.; Mottley, C.; Mann, L. C. *J. Am. Chem. Soc.* **1994**, *116*, 2171.

(10) (a) Lambert, C.; Nöll, G.; Schelter, J. *Nat. Mater.* **2002**, *1*, 69. (b) Brunschwig, B. S.; Creutz, C.; Sutin, N. *Chem. Soc. Rev.* **2002**, *31*, 168. (c) Londergan, C. H.; Kubaik, C. P. *J. Phys. Chem. A* **2003**, *107*, 9301. (d) Lambert, C.; Amthor, S.; Schelter, J. *J. Phys. Chem. A* **2004**, *108*, 6474. (e) D'Alessandro, D. M.; Keene, F. R. *Chem. Soc. Rev.* **2006**, *35*, 424. (f) Lear, B. J.; Chisholm, M. H. *Inorg. Chem.* **2009**, *48*, 10954.

(11) Launay, J.-P.; Coudret, C.; Hortholary, C. *J. Phys. Chem. B* **2007**, *111*, 6788.

(12) (a) Salsman, J. C.; Ronco, S.; Londergan, C. H.; Kubiak, C. P. *Inorg. Chem.* **2006**, *45*, 547. (b) Goeltz, J. C.; Benson, E. E.; Kubiak, C. P. *J. Phys. Chem. B* **2010**, *114*, 14729. (c) Glover, S. D.; Kubiak, C. P. *J. Am. Chem. Soc.* **2011**, *133*, 8721. (d) Kubiak, C. P. *Inorg. Chem.* **2013**, *52*, 5663.

(13) (a) Fox, M. A.; Le Guennic, B.; Roberts, R. L.; Brue, D. A.; Yufit, D. S.; Howard, J. A. K.; Manca, G.; Halet, J.-F.; Hartl, F.; Low, P. J. *J. Am. Chem. Soc.* **2011**, *133*, 18433. (b) Parthey, M.; Gluyas, J. B. G.; Fox, M. A.; Low, P. J.; Kaupp, M. *Chem.—Eur. J.* **2014**, *20*, 6895.

(14) (a) Yao, C.-J.; Sui, L.-Z.; Xie, H.-Y.; Xiao, W.-J.; Zhong, Y.-W.; Yao, J. *Inorg. Chem.* **2010**, *49*, 8347. (b) Wang, L.; Yang, W.-W.; Zheng, R.-H.; Shi, Q.; Zhong, Y.-W.; Yao, J. *Inorg. Chem.* **2011**, *50*, 7074.

(15) (a) Yao, C.-J.; Zhong, Y.-W.; Nie, H.-J.; Abruña, H. D.; Yao, J. *J. Am. Chem. Soc.* **2011**, *133*, 20720. (b) Yao, C.-J.; Yao, J.; Zhong, Y.-W. *Inorg. Chem.* **2012**, *51*, 6259.

(16) (a) Duprez, V.; Launay, J.-P.; Gourdon, A. *Inorg. Chim. Acta* **2003**, *343*, 395. (b) Yang, W.-W.; Yao, J.; Zhong, Y.-W. *Organometallics* **2012**, *31*, 1035. (c) Djukic, J.-P.; Sortais, J.-B.; Barloy, L.; Pfeffer, M. *Eur. J. Inorg. Chem.* **2009**, 817. (d) Jäger, M.; Smeigh, A.; Lombeck, F.; Görls, H.; Collin, J.-P.; Sauvage, J.-P.; Hammarström, L.; Johannsson, O. *Inorg. Chem.* **2010**, *49*, 374. (e) Wadman, S. H.; Lutz, M.; Tooke, D. M.; Spek, A. L.; Hartl, F.; Havenith, R. W. A.; van Klink, G. P. M.; van Koten, G. *Inorg. Chem.* **2009**, *48*, 1887. (f) Koivisto, B. D.; Robson, K. C. D.; Berlinguette, C. P. *Inorg. Chem.* **2009**, *48*, 9644. (g) Yao, C.-J.; Nie, H.-J.; Yang, W.-W.; Shao, J.-Y.; Yao, J.; Zhong, Y.-W. *Chem.—Eur. J.* **2014**, *20*, 17466.

(17) (a) Yang, W.-W.; Zhong, Y.-W.; Yoshikawa, S.; Shao, J.-Y.; Masaoka, S.; Sakai, K.; Yao, J.; Haga, M.-a. *Inorg. Chem.* **2012**, *51*, 890. (b) Yang, W.; Zhong, Y. *Chin. J. Chem.* **2013**, *31*, 329.

(18) Yao, C.-J.; Yao, J.; Zhong, Y.-W. *Inorg. Chem.* **2011**, *50*, 6847.

(19) Zhang, Y.-M.; Shao, J.-Y.; Yao, C.-J.; Zhong, Y.-W. *Dalton Trans.* **2012**, *41*, 9280.

(20) Crystallographic data for $\mathbf{4}(PF_6)_2$ (CCDC: 985947): dark red crystal, $C_{66}H_{42}F_{12}N_{10}P_2Ru_2$, M = 1467.18, triclinic, space group P-1, a = 8.6930(17) Å, b = 14.029(3) Å, c = 15.207(3) Å, α = 76.71(3)°, β = 79.72(3)°, γ = 76.24(3)°, U = 1738.0(6) Å^3, T = 173 K, Z = 1, 6321 reflections measured, radiation type Mo Kα, radiation wavelength 0.71073 Å, final R indices R1 = 0.0721, wR2 = 0.1700, R indices (all data) R1 = 0.0894, wR2 = 0.1828.

(21) Cui, B.-B.; Shao, J.-Y.; Zhong, Y.-W. *Organometallics* **2014**, *33*, 4220.

(22) Wadman, S. H.; Havenith, R. W. A.; Hartl, F.; Lutz, M.; Spek, A. L.; van Klink, G. P. M.; van Koten, G. *Inorg. Chem.* **2009**, *48*, 5685.

(23) (a) Concepcion, J. J.; Dattelbaum, D. M.; Meyer, T. J.; Rocha, R. C. *Philos. Trans. R. Soc. A* **2008**, *366*, 163. (b) Demadis, K. D.; Hartshorm, C. M.; Meyer, T. J. *Chem. Rev.* **2001**, *101*, 2655. (c) Nie, H.-J.; Shao, J.-Y.; Yao, C.-J.; Zhong, Y.-W. *Chem. Commun.* **2014**, *50*, 10082.

(24) Winter, R. F. *Organometallics* **2014**, *33*, 4517.

(25) (a) Risko, C.; Barlow, S.; Coropceanu, V.; Halik, M.; Bredas, J.-L.; Marder, S. R. *Chem. Commun.* **2003**, 194. (b) Bailey, S. E.; Zink, J. I.; Nelsen, S. F. *J. Am. Chem. Soc.* **2003**, *125*, 5939. (c) Bencini, A.; Ciofini, I.; Daul, C. A.; Ferretti, A. *J. Am. Chem. Soc.* **1999**, *121*, 11418.

DOI: 10.1021/ic503117k
Inorg. Chem. 2015, 54, 4688−4698

(26) (a) Vacher, A.; Barrière, F.; Roisnel, T.; Piekara-Sady, L.; Lorcy, D. *Organometallics* **2011**, *30*, 3570. (b) Mahapatra, A. K.; Datta, S.; Goswami, S.; Mukherjee, M.; Mukherjee, A. K.; Chakravorty, A. *Inorg. Chem.* **1986**, *25*, 1715. (c) Munshi, P.; Samanta, R.; Lahiri, G. K. *J. Organomet. Chem.* **1999**, *586*, 176. (d) Kannan, S.; Kumar, K. N.; Ramesh, R. *Polyhedron* **2008**, *27*, 701.

(27) (a) Patra, S.; Sarkar, B.; Mobin, S. M.; Kaim, W.; Lahiri, G. K. *Inorg. Chem.* **2003**, *42*, 6469. (b) Kasack, V.; Kaim, W.; Binder, H.; Jordanov, J.; Roth, E. *Inorg. Chem.* **1995**, *34*, 1924. (c) Chanda, N.; Sarkar, B.; Kar, S.; Fiedler, J.; Kaim, W.; Lahiri, G. K. *Inorg. Chem.* **2004**, *43*, 5128.

(28) Frisch, M. J.; Trucks, G. W.; Schlegel, H. B.; Scuseria, G. E.; Robb, M. A.; Cheeseman, J. R.; Montgomery, J. A.; Vreven, T., Jr.; Kudin, K. N.; Burant, J. C.; Millam, J. M.; Iyengar, S. S.; Tomasi, J.; Barone, V.; Mennucci, B.; Cossi, M.; Scalmani, G.; Rega, N.; Petersson, G. A.; Nakatsuji, H.; Hada, M.; Ehara, M.; Toyota, K.; Fukuda, R.; Hasegawa, J.; Ishida, M.; Nakajima, T.; Honda, Y.; Kitao, O.; Nakai, H.; Klene, M.; Li, X.; Knox, J. E.; Hratchian, H. P.; Cross, J. B.; Adamo, C.; Jaramillo, J.; Gomperts, R.; Stratmann, R. E.; Yazyev, O.; Austin, A. J.; Cammi, R.; Pomelli, C.; Ochterski, J. W.; Ayala, P. Y.; Morokuma, K.; Voth, G. A.; Salvador, P.; Dannenberg, J. J.; Zakrzewski, V. G.; Dapprich, S.; Daniels, A. D.; Strain, M. C.; Farkas, O.; Malick, D. K.; Rabuck, A. D.; Raghavachari, K.; Foresman, J. B.; Ortiz, J. V.; Cui, Q.; Baboul, A. G.; Clifford, S.; Cioslowski, J.; Stefanov, B. B.; Liu, G.; Liashenko, A.; Piskorz, P.; Komaromi, I.; Martin, R. L.; Fox, D. J.; Keith, T.; Al-Laham, M. A.; Peng, C. Y.; Nanayakkara, A.; Challacombe, M.; Gill, P. M. W.; Johnson, B.; Chen, W.; Wong, M. W.; Gonzalez, C.; Pople, J. A. *Gaussian 09*, revision A.2; Gaussian, Inc.: Wallingford, CT, 2009.

(29) Lee, C.; Yang, W.; Parr, R. G. *Phys. Rev. B* **1988**, *37*, 785.

(30) Hay, P. J.; Wadt, W. R. *J. Chem. Phys.* **1985**, *82*, 299.

(31) Dunning, T. H.; Hay, P. J. In *Modern Theoretical Chemistry*; Schaefer, H. F., Ed.; Plenum: New York, 1976; Vol. 3, p 1.

(32) Barone, V.; Cossi, M. *J. Phys. Chem. A* **1998**, *102*, 1995.

(33) (a) Mücke, P.; Linseis, M.; Záliš, S.; Winter, R. F. *Inorg. Chem. Acta* **2011**, *374*, 36. (b) Remenyi, C.; Kaupp, M. *J. Am. Chem. Soc.* **2005**, *127*, 11399. (c) Kowalski, K.; Linseis, M.; Winter, R. F.; Zabel, M.; Záliš, S.; Kelm, H.; Krüger, H.-J.; Sarkar, B.; Kaim, W. *Organometallics* **2009**, *28*, 4196. (d) Fox, M. A.; Roberts, R. L.; Baines, T. E.; Le Guennic, B.; Halet, J.-F.; Hartl, F.; Yufit, D. S.; Albesa-Jové, D.; Howard, J. A. K.; Low, P. J. *J. Am. Chem. Soc.* **2008**, *130*, 3566.

(34) Hardesty, J.; Goh, S. K.; Marynick, D. S. *J. Mol. Struct: THEOCHEM* **2002**, *588*, 223.

(35) Yokogawa, D.; Sato, H.; Nakao, Y.; Sakaki, S. *Inorg. Chem.* **2007**, *46*, 1966.

(36) Yanai, T.; Tew, D. P.; Handy, N. C. *Chem. Phys. Lett.* **2004**, *393*, 51.

(37) (a) Kundu, T.; Schweinfurth, D.; Sarkar, B.; Mondal, T. K.; Fiedler, J.; Mobin, S. M.; Puranik, V. G.; Kaim, W.; Lahiri, G. K. *Dalton Trans.* **2012**, *41*, 13429. (b) Das, A.; Kundu, T.; Mobin, S. M.; Priego, J. L.; Jimenez-Aparicio, R.; Lahiri, G. K. *Dalton Trans.* **2013**, *42*, 13733.

DOI: 10.1021/ic503117k
Inorg. Chem. 2015, 54, 4688−4698